CrossMark

JƒM PAPERS

Hydrodynamics of finite-length pipes at intermediate Reynolds numbers

Olivia Pomerenk[1], **Simon Carrillo Segura**[2], **Fangning Cao**[1], **Jiajie Wu**[1] and **Leif Ristroph**[1],†

[1]Applied Math Lab, Courant Institute of Mathematical Sciences, New York University, New York, NY 10012, USA

[2]Department of Mechanical and Aerospace Engineering, Tandon School of Engineering, New York University, Brooklyn, NY 11201, USA

Extensive studies of the hydraulics of pipes have focused on limiting cases, such as fully-developed laminar or turbulent flow through long conduits and the accelerating flow through an orifice, for which there exist laws relating pressure drop and flow rate. We carry out experiments on smooth, circular pipes for dimensions and flow rates that interrogate intermediate conditions between the well-studied limits. Organizing this information in terms of dimensionless friction factor, Reynolds number and pipe aspect ratio yields a surface $f_D(Re, \alpha)$ that is shown to match the three laws associated with developed laminar, developed turbulent, and orifice flows. While each law fails outside its applicable range of (Re, α), we present a hybrid theoretical–empirical model that includes inlet, development and transition effects, and that proves accurate to approximately 10 % over wide ranges of Re and α. We also present simple formulas for the boundaries between the three hydraulic regimes, which intersect at a triple point. Measurements show that sipping through a straw is an everyday example of such intermediate conditions not accounted for by existing laws but described accurately by our model. More generally, our findings provide formulas for predicting frictional resistance for intermediate-Re flows through finite-length pipes.

Key words: pipe flow boundary layer, transition to turbulence, pipe flow

1. Introduction

Flow through a pipe is an archetypal problem due to its prevalence in many natural contexts and engineering applications, as well as in everyday situations such as drinking through a straw. Certain limiting cases greatly simplify the relevant considerations and analysis, leading to classical laws of hydraulics that relate the pressure difference to the

† Email address for correspondence: ristroph@cims.nyu.edu

flow rate (Reynolds 1883; Moody 1944; Acheson 1991; Batchelor & Batchelor 2000; Mullin 2011; White 2011). The famous Hagen–Poiseuille law is a linear pressure-flow relation that applies to developed laminar and viscous flow through sufficiently long pipes and at sufficiently low Reynolds numbers *Re*. In the presence of disturbances, the flow transitions to turbulence near *Re* = 2000 (Reynolds 1883; Moody 1944; Acheson 1991; Draad, Kuiken & Nieuwstadt 1998; Batchelor & Batchelor 2000; Kerswell 2005; Ben-Dov & Cohen 2007; Mullin 2011; White 2011), and developed turbulent flow in long pipes leads to a nonlinear pressure-flux relation that has been characterized empirically across high *Re* (Colebrook *et al.* 1939; Moody 1944; Nikuradse 1950; Adams, Grant & Watson 2012).

The classical laws for laminar and turbulent flow break down in short pipes due to entrance effects associated with the developing flow (Fargie & Martin 1971; White 2011; Malcherek 2016). The hydrodynamic entrance length is well characterized across flow regimes, and the consequences for the pressure-flux relation have been investigated for both laminar and turbulent flows (Sparrow, Lin & Lundgren 1964; Wang & Tullis 1974; Acheson 1991; Dombrowski *et al.* 1993; Batchelor & Batchelor 2000; White 2011; Langhaar 2021). Very short pipes – the extreme of which is an orifice – involve inertial effects associated with the converging and accelerating inlet flow. The hydraulics of such cases are better described by modifications of Torricelli's law involving a geometry- and *Re*-dependent discharge coefficient (Semat & Katz 1958; Wu, Burton & Schoenau 2002; White 2011; Ferrante 2012).

For the more general problem of flow of arbitrary rate through a smooth-walled pipe of arbitrary length, it would be convenient and useful if the various factors reviewed above were united and organized within a common framework. For example, given a set of parameters, one would like to be able to quickly assess which, if any, of the classical pipe flow regimes is applicable. It would also be valuable to have approximate but sufficiently accurate pressure-flux formulas that would apply generally to pipes of finite length and for flow rates that induce conditions between the well-studied limits. In this work, we pursue these goals for the case of pressure-driven flow through straight, rigid pipes with smooth walls and circular cross-section. We frame our work in the context of drinking through a straw and similar forms of tubular drinking by animals, which is relatable and thus pedagogically useful. Moreover, while straw drinking is commonly cited as an everyday example governed by the Hagen–Poiseuille law, we show that it in fact epitomizes the conditions for which no classical law applies. We seek an improved accounting of the hydraulics for such intermediate-Reynolds-number flows through intermediate-length pipes.

2. Dimensional and scaling analyses, and the pipe flow map

An organizing framework is naturally suggested by a dimensional analysis of the problem of flow through a smooth, circular pipe. As illustrated schematically in figure 1(*a*), the relevant physical parameters involved are the pipe length *L* and inner diameter *D*, the fluid density ρ and viscosity μ, the mean flow speed *U*, and the pressure difference Δp. These six quantities may be viewed as one dependent and five independent variables, e.g. $\Delta p(L, D, \rho, \mu, U)$. The five independent dimensional quantities can be reduced to two dimensionless groups by employing the Buckingham Pi theorem and noting that the three dimensions of mass, length and time are involved (Curtis, Logan & Parker 1982). The dependent quantity may also be non-dimensionalized, yielding in total three dimensionless groups with any one being viewed as a function of the others. Following common conventions, we select the flow Reynolds number $Re = \rho U D / \mu$ and the pipe aspect ratio $\alpha = L/D$ as independent variables that dictate the Darcy friction factor
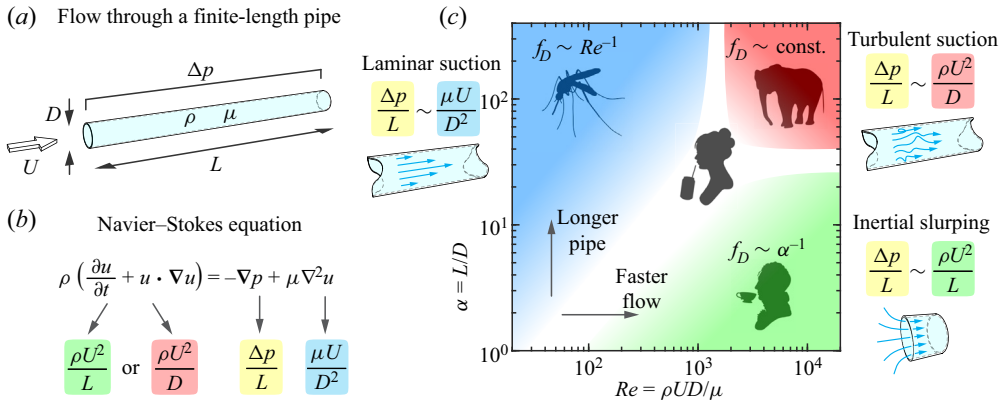
Figure 1. An organizing framework for pipe flows. (*a*) Relevant variables. The pipe length L and inner diameter D, the fluid density ρ and viscosity μ, and the flow speed U dictate the pressure drop $\Delta p = \Delta p(L, D, \rho, \mu, U)$. (*b*) Scaling of terms in the Navier–Stokes equation. The applied pressure gradient (yellow) balances viscous (blue) and inertial (green and red) stresses, each of which follows a simple scaling. (*c*) Map of pipe flow regimes in the space of Reynolds number Re and pipe aspect ratio α. Three classical regimes of developed laminar, developed turbulent, and undeveloped inlet flows are associated with distinct domains of (Re, α). Each regime involves the applied pressure gradient predominantly balancing one other scaling term.

$f_D = 2\Delta p D / \rho U^2 L$. The latter is a dimensionless form of pressure drop whereby the applied gradient $\Delta p / L$ is scaled by the inertial term $\rho U^2 / 2D$ relevant to well-developed turbulence (Acheson 1991; White 2011). Hence all cases of pipe flow are encompassed by a function $f_D(Re, \alpha)$.

The classical limits correspond to regimes of (Re, α) that can be interpreted through a scaling analysis of terms in the governing Navier–Stokes equation. As shown in figure 1(*b*), the equation can be understood as a balance of the applied pressure gradient (yellow) with inertial (green and red) and viscous (blue) effects, each of which satisfies a scaling relation with the dimensional variables. We assert that the well-studied limits of pipe flow correspond to this balance being dictated principally by the applied gradient overcoming only one such effect, with the others playing negligibly small roles. For example, the applied gradient $\Delta p / L$ balances viscous resistance $\mu U / D^2$ for developed laminar flow, yielding the Hagen–Poiseuille law that applies for sufficiently slow flow through long, slender pipes, i.e. low Re and high α. Expressed in non-dimensional form, $f_D \sim Re^{-1}$ with no dependence on α. As indicated in the blue region of figure 1(*c*), a mosquito drinking through its proboscis serves as a mascot of such laminar suction (Kim & Bush 2012). Classical pipe flow turbulence corresponds to a balance of $\Delta p / L$ with inertial gradients $\rho U^2 / D$ transverse to the pipe axis, which applies to fast flows and slender pipes, i.e. high Re and high α. The dimensionless form is $f_D \sim$ const., independent of both Re and α. An elephant drawing water into its trunk might satisfy such turbulent suction (red). A third regime is associated with Torricelli's law for flow through an orifice or very short pipe, i.e. low α, in which case $\Delta p / L$ is invested in overcoming the inertial gradient $\rho U^2 / L$ along the pipe axis. The dimensionless form is $f_D \sim \alpha^{-1}$, independent of Re. This regime might be termed inertial slurping (green) and may relate to drinking tea or soup through pursed lips, which can be viewed crudely as forming a very short pipe.

A main result to be shown in this work is that the regimes have an interesting structure in which their dividing boundaries meet at a triple-point-like region. Moreover, the typical values of Re and α during sipping through a straw will be shown to sit near this region, as indicated by the soda drinker in figure 1(*c*). Hence, while straw drinking
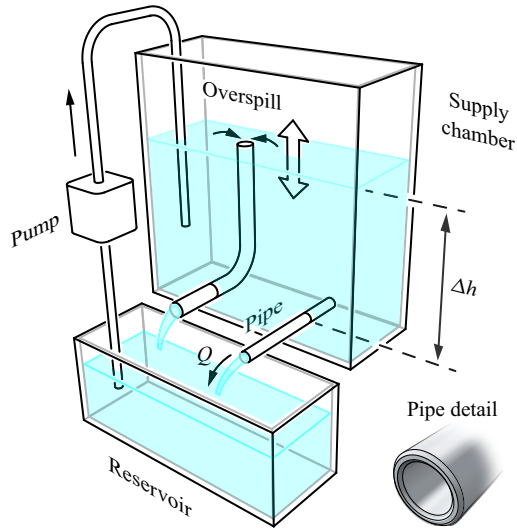
Figure 2. Apparatus for hydraulic characterization of pipes and straws. Flow through a pipe is driven by the hydrostatic pressure associated with the depth Δh. The liquid level in the supply chamber is maintained by an overspill system consisting of a pump from a reservoir and an internal drain, whose height can be adjusted via a translation stage (represented by the arrow) in order to sweep through values of Δh. The volumetric flux Q is measured by timing the collection of liquid within a beaker or graduated cylinder (not shown). The inset shows the chamfering applied to the inlet and outlet of all pipes.

differs from the idealized pipe flow problem studied here, this everyday experience can serve as a mnemonic for the 'lawless' borderlands between the well-studied hydraulic regimes and where the conventional relations therefore do not apply. This context also motivates the development of a universal hydraulic model that is informed by and validated against experimental measurements, and that spans the regimes and furnishes approximate pressure-rate relations applicable to intermediate cases.

3. Experiments

We carry out hydraulic measurements on pipes using an experimental system that allows for the exploration of wide ranges of Re and α. We specifically interrogate intermediate values of Re and α that are between and somewhat into the classical regimes. The apparatus is a customized version of the commonly used scheme in which constant hydrostatic pressure drives flow through a conduit, and the flux or volumetric flow rate is measured. As shown in figure 2, the major components include a large tank that supplies the liquid, a reservoir into which the pipe drains, and an overspill system that maintains the water level in the supply chamber. The latter involves a pump whose rate is adjusted to be just higher than the flux lost through the pipe, the excess returning to the reservoir through an internal drain. The hydrostatic pressure difference $\Delta p = \rho g \Delta h$ is controlled and varied via a translation stage (not shown in figure 2, but symbolized by an arrow) that sets the height Δh of the internal drain relative to the pipe. Here, ρ is the density of the liquid, which is water and water–glycerol mixtures for these experiments. A given pipe is inserted through a hole in the chamber wall and secured via an external fitting. The liquid level in the supply chamber is monitored with a ruler and recorded after equilibration. The volumetric flow rate Q is then measured by timing with a stopwatch the collection of a targeted volume in a precision beaker or graduated cylinder that intercepts the efflux from the pipe.

We intend this experimental setting to target an idealized pipe flow problem that relates to and informs on tubular drinking but differs in several respects. Our focus is on smooth, rigid, straight pipes of circular cross-section, whereas the geometries of real straws and other conduits are more varied. Although liquid is typically raised against gravity during drinking, fixing the pipe horizontally isolates the hydrodynamic component of the problem. We impose a constant differential pressure and measure the mean flow rate over long times; an alternative would impose the rate and measure pressure. In contrast, drinking involves variations of pressure and flow. We will explore a sufficiently broad range of pressures and rates to cover typical drinking conditions (Nilsson *et al.* 1996). The inlet condition adopted here involves drawing from a reservoir large enough to approximate quiescent fluid in the far field, which is an idealization of a straw or tube well away from the boundaries of a container. The outlet condition is a jet of liquid open to the atmosphere, whereas in straw drinking, the mouth is filled with air and liquid whose proportions change during a sip.

We assess 41 pipes made from high-polish stainless steel of inner diameters $D \in [0.1, 0.8]$ cm and lengths $L \in [2, 90]$ cm. The inlet and outlet edges are machined flat and then chamfered internally and externally (inset of figure 2). The length, height and width of the supply tank measure 40 cm × 40 cm × 20 cm, chosen to be much larger than the pipe diameters. The overspill drain and pump input tube are located in the tank at the opposite end from the pipe in order to minimize flow disturbances. Each pipe is tested for approximately 10 values of $\Delta h \in [1, 30]$ cm using pure water near room temperature, and we measure Q three times to ensure reproducibility. The mean Q for each condition is converted to a mean speed $U = Q/A$ across the pipe cross-section of area $A = \pi D^2/4$. The data are cast in terms of the Reynolds number $Re = \rho U D/\mu$, aspect ratio $\alpha = L/D$, and friction factor $f_D = 2\Delta p D/\rho U^2 L$. Lower values of Re are attained for some pipes using two water–glycerol mixtures, whose density ρ and viscosity μ are measured with a precision digital balance and ball viscometer, respectively. Temperature is monitored continuously and found to vary by at most $1\,^{\circ}\text{C}$ during each experiment for a given pipe and given fluid. The mean temperature is then used in the computation of the kinematic viscosity and thus Re for the corresponding data set.

The entire set of measurements $f_D(Re, \alpha)$ is presented as markers in figure 3, where figure 3(*a*) shows the range and density of the data in the (Re, α) parameter space, and figure 3(*b*) provides a three-dimensional view. These plots are intended to introduce the scope and general character of the data, which comprise 697 total measurements spanning $Re \in [30, 10\,000]$, $\alpha \in [2, 200]$ and $f_D \in [0.04, 3]$. All data are available in the supplementary spreadsheet available at https://doi.org/10.1017/jfm.2023.99. The faces of the markers in figure 3(*a*) are coloured according to the measured f_D (see colour bar), and each horizontal array of data points corresponds to a specific pipe tested for a specific liquid. The background colour of figure 3(*a*) and the coloured surface of figure 3(*b*) represent the predictions of a model that will be developed in the next section.

To better reveal the trends, subsets of the data corresponding to horizontal and vertical transects in the space of (Re, α) are shown in the plots of figures 3(*c,d*). The curves are representative of high α and high Re, respectively, for which portions of the data are expected to align with the classical laws of pipe flow. For example, figure 3(*c*) considers $\alpha = 100$ (see inset), which ought to be large enough that the Hagen–Poiseuille law for laminar flow applies at lower Re, and turbulent effects dominate at higher Re. In the appropriate limits, the measurements (markers) indeed follow trends consistent with classical laws (dashed blue and red curves), the forms of which will be discussed in detail below. Our model (black curve) gives better correspondence across the entire range of
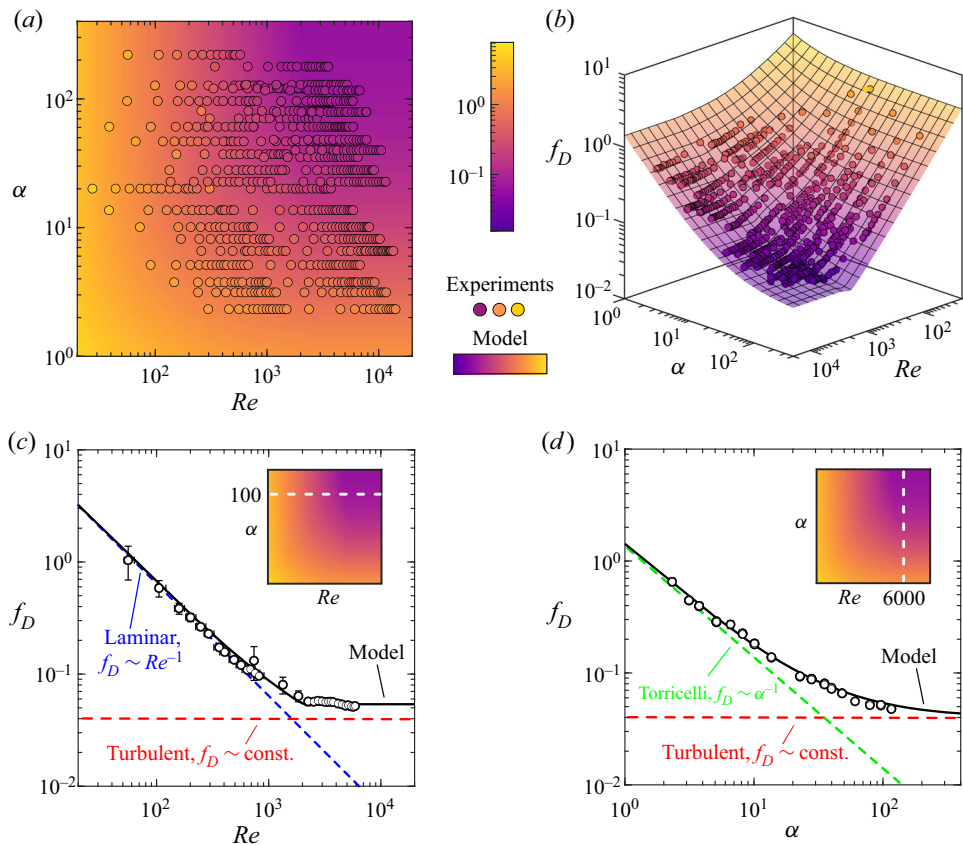
Figure 3. Master plots of pipe flow hydraulics with experimental measurements (markers) and model (coloured surface). (a) A view of the (Re, α) parameter space, with f_D displayed as the marker face colour for experiments and the background colour for the model. The two show strong agreement across most of the space. (b) A three-dimensional view of the entire surface $f_D(Re, \alpha)$. (c) A transect at a fixed and high value of $\alpha = 100$. The data correspond to a single pipe tested across a range of pressures for pure water and a water–glycerol mixture, and error bars are described in the text. Also shown are dashed blue and red curves that correspond to the classical laws for developed laminar and turbulent flow, respectively. The black curve indicates the results of the current model. (d) A transect at a fixed and high value of $Re = 6000 \pm 500$, where the experimental data correspond to many different pipes tested for pure water. Error bars are typically smaller than the symbol size. Also shown are curves for the laws of Torricelli (dashed green), turbulence (dashed red) and the current model (solid black).

Re. Similarly, figure 3(d) considers high $Re = 6000$ (see inset), for which the expectation of developed turbulent flow for large α is corroborated by the measurements. Very short pipes of low α are more consistent with a Torricelli-like law (dashed green curve), and our model agrees well with the data across all α.

The experimental data of figures 3(c,d) include error bars, which are generally smaller than the marker size. The errors in α are negligibly small, as the pipe diameters are provided with tight tolerance and the lengths are measured accurately. Errors in Re are computed based on the standard deviation of the three measurements of Q, whose variability is kept small by always collecting the pipe efflux over times of 40 s or longer. The error bars prove to be smaller than the symbol size for almost all the data of figures 3(c,d), and relative errors in Re are typically 1 % and at worst 10 %. The errors

in f_D are associated predominantly with the pipe-to-surface height Δh that appears in the calculation of the pressure. The location of the water surface can be measured with a precision of approximately 1 mm, and the depth of each pipe is taken as determined with an error equal to its radius. These effects compound to give relative errors that are generally under 5 % but can be as great as 30 %, which occurs only for the lowest values of Δh in a given pipe–fluid data set.

4. Hydraulic model formulation

Here, we present a model that aims to account for the hydraulics of pipes of differing aspect ratios subject to flows of differing rates and with the specific aim of spanning the classical regimes of pipe flow. The end goal is a universal function $f_D(Re, \alpha)$. We take a hybrid theoretical–empirical approach that unifies and combines the many previous characterizations of smooth pipe hydraulics and especially aspects of flows through orifices, in the entrance region, developing and developed laminar and turbulent states, and the laminar-to-turbulent transition. Whenever possible, we appeal to theory or observations when making the many choices about the model structure and parameter values. Other aspects are dictated by mathematical simplicity or convenience, such as functions that combine smoothly different effects and have been employed in related works (Churchill 1977; Colebrook *et al.* 1939; Brkić & Praks 2018). Our model takes the general form

$$f_D(Re, \alpha) = f_D^I(Re, \alpha) + g^L(Re)f_D^L(Re, \alpha) + g^T(Re)f_D^T(Re, \alpha), \tag{4.1}$$

where f_D^I, f_D^L and f_D^T are functions that capture the individual contributions to the friction factor that come from inlet effects, laminar flow, and turbulent flow, respectively. This structure is motivated by the fact that inlet effects contribute for all pipes at all conditions and thus across the space of (Re, α), whereas laminar and turbulent effects are unique and apply within distinct ranges of Re. Here, $g^{L,T}(Re)$ are selection functions that take the value unity for Re deep within the laminar and turbulent regimes, respectively, and zero elsewhere. We use logistic functions for this purpose, which behave like smoothed Heaviside or step functions:

$$g^T(Re) = \frac{1}{1 + \exp(-(Re - Re^*)/\delta)}$$

and

$$g^L(Re) = 1 - g^T(Re) = \frac{1}{1 + \exp((Re - Re^*)/\delta)}. \tag{4.2a,b}$$

Here, Re^* is the critical Reynolds number at the laminar-to-turbulent transition, and δ can be interpreted as the width or range of Re over which the transition occurs. The parameter value $Re^* = 2000$ is consistent with the literature on the transition in the presence of sufficiently strong disturbances. The choice $\delta = 200$ is shown below to yield an acceptable match to the experimental data.

We next set about defining the contributing frictional terms, starting with inlet effects. In the short-pipe or orifice limit $\alpha \to 0$, acceleration effects dominate and the applied pressure gradient is invested in axial inertial gradients $\Delta p/L \sim \rho U^2/L$, corresponding to the green region of figure 1(*c*). The leading-order hydraulics is that of an ideal, inviscid fluid as described by Bernoulli's principle and Torricelli's law, which takes the form $\Delta p = \rho U^2/2$ or, equivalently, $f_D = 1/\alpha$ (Semat & Katz 1958; Fargie & Martin 1971; White 2011; Malcherek 2016). The actual efflux velocity is somewhat lower due to streamline contraction and viscous effects. These complexities determine the discharge

coefficient $C_D \leq 1$ or ratio of actual-to-ideal efflux speed, whose value depends on Re and the geometric details of the orifice (Wu *et al.* 2002; Ferrante 2012; Hicks & Slaton 2014). We assume a constant $C_D = 0.85$ and thus $f_D^I = 1/C_D^2 \alpha$. The parameter value is within the broad range 0.6–1.0 reported in previous studies, and is chosen to account satisfactorily for the low-α portion of our experimental data set.

An accounting of the laminar flow contribution f_D^L must include the developed flow far down the pipe as well as the developing flow in the entrance region. For sufficiently low Re and high α, the developed laminar flow involves the applied pressure balancing viscous stress, $\Delta p/L \sim \mu U/D^2$, corresponding to the blue region of figure 1(*c*). The developed flow profile is parabolic, and the hydraulics is described by the Hagen–Poiseuille law $\Delta p = 32\mu LU/D^2$, which is equivalent to $f_D = 64/Re$ (Stokes 1845; Acheson 1991; Batchelor & Batchelor 2000; White 2011). Viscous and inertial effects lead to an enhanced pressure drop in the entrance region over which the flow develops. Previous works have shown that the cumulative pressure drop coefficient $2\Delta p(x)/\rho U^2$ increases with the streamwise coordinate x before saturating at an order-1 value for x much larger than the hydrodynamic entrance length L_E (Sparrow *et al.* 1964; Langhaar 2021). Associating x with L and recasting in terms of α yields $f_D(\alpha) = b(\alpha)/\alpha$, where $b(0) = 0$ and $b \to b_\infty$ for $x \gg L_E$. We assume an exponential form for b and adopt the empirical formula $L_E = k \, Re \, D$ for the length at which the flow profile is within 99 % of the developed parabolic profile, where $k = 0.05$ (Acheson 1991; Dombrowski *et al.* 1993; Batchelor & Batchelor 2000; White 2011). Hence the friction contributions from developing and developed laminar flow are given by

$$f_D^L = \frac{b_\infty}{\alpha} \left(1 - \exp(-\alpha \ln 100/k \, Re)\right) + \frac{64}{Re}, \tag{4.3}$$

where $b_\infty = 1$ is a simple choice that will be shown to yield satisfactory agreement with the experimental data. Previous theoretical studies indicate values in the range 1.2–1.4, while experiments are consistent with somewhat lower values, 1–1.2 (Campbell & Slattery 1963; Sparrow *et al.* 1964; Langhaar 2021).

Finally, we take up the turbulent flow contribution applicable to sufficiently high Re. Well-developed turbulence for long pipes or high α involves a balance of the applied pressure gradient with inertial gradients transverse to the pipe, corresponding to $\Delta p/L \sim \rho U^2/D$, which yields uniformly constant f_D for the red region of figure 1(*c*). Extensive characterizations have shown that $f_D \sim O(0.01)$ and f_D varies weakly with Re (Colebrook *et al.* 1939; Moody 1944; Nikuradse 1950; Langelandsvik, Kunkel & Smits 2008; White 2011; Adams *et al.* 2012). Flow development effects in the turbulent regime have been shown to be confined to a relatively short entrance region whose length $L_E/D \sim O(10)$ is insensitive to Re (Barbin & Jones 1963; Wang & Tullis 1974). The enhanced pressure drops due to development and inlet effects occur in the same region of the pipe and are thus not clearly distinguishable, and we make the simplifying assumption that the former leads to no additional contribution. Hence our model for the turbulent regime considers only fully developed flow, which is associated with a constant $f_D^T = f_D^* = 0.04$ that is representative of previously measured values 0.03–0.05 for $Re = 2000$–$10\,000$ (Moody 1944; Langelandsvik *et al.* 2008; White 2011; Adams *et al.* 2012).

In summary, the complete model has the form

$$f_D(Re, \alpha) = \frac{1}{C_D^2 \alpha} + \frac{1}{1 + \exp((Re - Re^*)/\delta)} \left[\frac{b_\infty}{\alpha} (1 - \exp(-\alpha \ln 100/k\,Re)) + \frac{64}{Re} \right]$$

$$+ \frac{1}{1 + \exp(-(Re - Re^*)/\delta)} f_D^*. \tag{4.4}$$

The six parameters and their values are $C_D = 0.85$, $Re^* = 2000$, $\delta = 200$, $b_\infty = 1$, $k = 0.05$ and $f_D^* = 0.04$.

5. Model results, comparison to experiments, and drinking straws

Here, we compare the model results to experimental measurements of pipes and drinking straws, and also use the model to interpret the hydraulic regimes and their boundaries.

5.1. *Model results and comparison to experiments*

The model prediction for $f_D(Re, \alpha)$ is presented as the coloured background in figure 3(*a*), and comparison to the face colour of the markers shows good qualitative agreement with the experimental measurements. The same model output is shown as the coloured surface of figure 3(*b*), where good correspondence with experiments is confirmed. The transects of figures 3(*c*,*d*) allow for a closer comparison, and the model predictions (black curves) show strong agreement with the measurements (markers). Also shown are dashed coloured curves representing the classical laws associated with Torricelli (green), developed laminar flow (blue) and developed turbulence (red). The respective formulas for f_D are $1/C_D^2 \alpha$, $64/Re$ and f_D^*, as detailed in the previous section. These laws provide good matches to the data only in the appropriate limits of Re and α, whereas our model furnishes accurate predictions across the entire range of parameter values. Particularly for intermediate values of $Re \in [500, 5000]$ and $\alpha \in [10, 100]$, all existing laws do not apply, while our model accounts accurately for the fluid friction.

For a quantitative comparison, we assess the relative deviation of the model predictions from the experimental measurements, that is, $[f_D^M(Re, \alpha) - f_D^E(Re, \alpha)]/f_D^E(Re, \alpha)$, where the superscript M and E indicate model and experiment. This quantity is shown in figure 4(*a*), where the face colour on the experimental markers indicates the deviation as a percentage. Here, cyan tones indicate that the model overpredicts the measured friction, and magenta indicates an underestimate. White marks those data with deviations under 10 %, which is satisfied by approximately 75 % of the points.

The mean of the relative deviations is under 1 %, and the standard deviation is 10 %. Deviations of this order are expected, since the model parameters C_D, Re^*, b_∞, k and f_D^* are each determined only at the 10–30 % level based on previous studies. (The quantity δ can be viewed as a mathematical fitting parameter with no clear basis in pipe flow phenomena.) Further, our experimental errors can reach 30 % for the lowest pressures and lowest Re for which a given pipe is tested with a given fluid. In light of these facts, the model can be seen as successfully furnishing predictions of accuracy of the order of 10 % for the hydrodynamic losses in finite-length pipes across intermediate Re.

5.2. *Classical regimes of pipe flow*

The classical pipe flow regimes can be understood as certain limits of the model. Very short conduits satisfy $\lim_{\alpha \to 0} f_D = f_D^I = 1/C_D^2 \alpha$, which is the inlet flow contribution
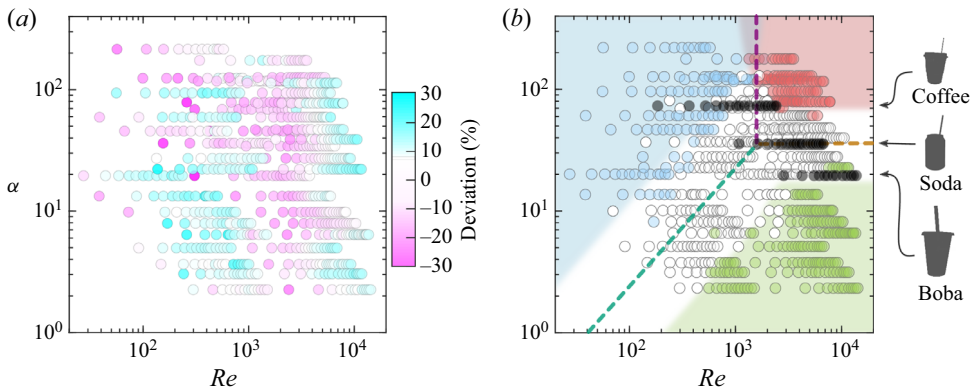
Figure 4. Comparison of experiments and model, identification of regime boundaries, and placement of drinking straws. (*a*) The signed deviation of the model predictions relative to experimental measurements. The deviations are largely unstructured in the parameter space, and typical mean squared values are under 10 %. (*b*) Regimes correspond to inlet (green), developed laminar (blue) and developed turbulent (red) flows. The data markers are coloured only if the experimentally measured friction is within 50 % of that predicted by the classical regime laws; they are white otherwise. The background is shaded via the same colour scheme for regions predicted by the model to lie within 50 % of these laws. The agreement of the marker and background colours indicates that the classical regimes are well identified. Boundaries (dashed lines) obtained by pairwise equating of the laws reveal a triple-point-like region. Three types of drinking straws are tested experimentally and found to reside near this point.

furnished by Torricelli's law modified with a discharge coefficient. In this limit of $\alpha \to 0$, the laminar contribution comes to $b_\infty \ln 100/k\,Re + 64/Re$ and hence is constant for any given Re, as is the turbulent contribution of f_D^*, whereas the inlet contribution diverges and is thus dominant. Developed flow of either kind corresponds to $\alpha \to \infty$, in which case the inlet contribution vanishes. Developed laminar flow corresponds to $\lim_{(Re,\alpha)\to(0,\infty)} f_D = 64/Re$, which is the dimensionless form of the Hagen–Poiseuille law. This is the second term of (4.3) for f_D^L and diverges in the limit, whereas the first term tends to zero. Developed turbulent flow is associated with $\lim_{(Re,\alpha)\to(\infty,\infty)} f_D = f_D^T = f_D^*$, as all other terms vanish. These results verify that the model, by its construction, recapitulates the classical laws of pipe flow hydraulics.

Evaluating the degree of correspondence between the experimental measurements and the three classical laws shows where in the (Re, α) space these laws apply. We form the difference of the measured $f_D(Re, \alpha)$ from the ideal forms $1/C_D^2\alpha$, $64/Re$ and f_D^* that apply within the inlet, laminar and turbulent regimes, respectively. In figure 4(*b*), we colour the faces of those markers that depart from the ideal forms by less than 50 %. Here, we maintain the colour coding from figure 1 that green, blue and red respectively signify the inlet, laminar and turbulent flow regimes. Their structure in the (Re, α) parameter space becomes yet more clear by carrying out the same analysis for the model, as shown by the background colouring. The results from both experiments and model justify the graphical summary of figure 1(*c*) showing the domains of the hydraulic regimes. While the classical laws apply formally for certain extremes in the parameter space, they prove to be good approximations over fairly broad regions.

5.3. *Boundaries separating the classical hydraulic regimes*

The classical hydraulic regimes are separated by boundary zones in which none of the laws provides accurate accounting of the frictional resistance. These 'lawless' borderlands

seem to lie along three lines in the space of (Re, α). The model provides simple formulas that approximate these boundaries by considering the conditions for which any pair of the limiting laws are equal. For example, the inlet–laminar boundary is found by equating $1/C_D^2\alpha = 64/Re$ and rearranging to reveal $\alpha = Re/64C_D^2$. This is the diagonal line (dashed, turquoise) on the log-log plot of figure 4(*b*). Similarly, the inlet–turbulent boundary is $1/C_D^2\alpha = f_D^*$ or $\alpha = 1/f_D^*C_D^2$, which is the horizontal line segment (brown). The laminar–turbulent boundary is given by $64/Re = f_D^*$ or $Re = 64/f_D^*$, which is the vertical line segment (violet). These simple formulas can be used to assess quickly within which sector of the (Re, α) space a given set of pipe flow conditions lies. They also determine the proximity to the boundaries, which can be used to justify or not the use of the corresponding limiting law.

The boundaries have clear interpretations in terms of pipe flow phenomena. The inlet–laminar diagonal line can be thought of as the set of conditions for which the pipe length is comparable to the entrance length for laminar flow. This is readily seen by noting that $L = L_E = k \, Re \, D$ is equivalent to $L/D = \alpha = k \, Re$, which is a diagonal line in the space of (Re, α). The coefficient $k = 0.05$ is comparable but somewhat greater than the value $1/64C_D^2 = 0.02$ obtained by our model prescription of the boundary, since the former corresponds to an entrance length based on the flow profile, and the latter is based on hydraulic contributions. Similarly, the inlet–turbulent horizontal line is a set of conditions for which the pipe length is comparable to the entrance length for turbulent flow. The common rules-of-thumb $L_E/D \approx 10$–40 (Nikuradse 1950; Wang & Tullis 1974; White 2011) are consistent with our prescription of the boundary as $\alpha = 1/f_D^*C_D^2 = 30$. Finally, the laminar–turbulent boundary is associated with the transition in flow at approximately $Re^* = 2000$, which matches the vertical boundary at $Re = 64/f_D^*$.

The scaling arguments of figure 1 offer a more general interpretation of each border as a set of conditions for which two of the principal fluidic stresses play more or less equal roles in determining the pressure drop. For example, the inlet–laminar boundary involves equal participation of the axial inertial pressure gradient and viscous stress in combining to balance the applied pressure gradient. Similarly, the inlet–turbulent boundary involves the combined effect of axial and transverse inertial gradients, and the laminar–turbulent boundary combines viscous effects and transverse inertial gradients.

5.4. *The hydraulic triple point and drinking straws*

The three boundaries intersect at a point that can be interpreted as a set of conditions in which all stresses in the Navier–Stokes equation participate more or less equally. This triple point is determined by our model boundaries to be $(Re, \alpha) = (64/f_D^*, 1/f_D^*C_D^2) \approx (2000, 30)$. It should be understood that there is a broader region in the vicinity of this point in which the full set of hydrodynamic complexities may arise.

Returning to drinking straws, it is curious that a standard soda straw has an aspect ratio that is quantitatively similar to the triple point value $\alpha \approx 30$. This motivates a hydraulic assessment of straws under the pressures and flow rates typical of human drinking. We collect and test three types of straws, including the slender type used as a coffee stirrer, the standard kind used for colas and soft drinks, and a large-diameter type used for boba or bubble tea. Measured values of the pressures generated in the human mouth overlap with those accessible in our apparatus (Nilsson *et al.* 1996). We thus test each straw over a range of pressures as done for the pipes, and the results are displayed as grey markers in figure 4(*b*). Strikingly, typical drinking conditions lie near the triple point. We view this correspondence as a curious coincidence but also a useful mnemonic:

straw sipping epitomizes the conditions that stir up all the hydrodynamic complexities of pipe flow and necessitate a model such as that presented here. These findings dispel the oft-repeated claim that drinking through a straw involves laminar flow governed by the Hagen–Poiseuille law (Eisenburger & Addy 2003; Pickover 2008; Vogel 2013).

6. Discussion and conclusions

This work provides a general framework for assessing and interpreting the hydraulics of flows at intermediate Reynolds numbers through smooth, circular pipes of intermediate aspect ratios. The resistance or friction factor across flow rates and pipe geometries is represented by a function $f_D(Re, \alpha)$, and experimental measurements are provided for regions in the parameter space that are between the well-studied limits of inlet or orifice flow, developed laminar flow, and developed turbulence. A model of the same is formulated by combining smoothly what is known empirically and theoretically about the classical regimes, flow development effects in the entrance region, and the laminar-to-turbulent transition. The model provides accurate estimates of the pressure drop for the intermediate conditions in which the conventional hydraulic laws do not apply. It also furnishes simple formulas for the boundaries between the regimes, which are useful for determining if a given set of conditions might be well approximated by a classical law or whether a more elaborate model such as ours is needed. Interestingly, these investigations also reveal that the three regimes are structured in the (Re, α) parameter space such that they meet at a triple-point-like region. Such conditions are maximally complex from a hydrodynamic perspective and yet commonplace, arising, for example, when sipping through a straw.

These results are useful conceptually and pedagogically as a scheme for uniting and organizing the various factors and phenomena involved in pipe flow. Effects associated with flow convergence and acceleration at inlets, profile development in the entrance region, and developed laminar and turbulent flows, are identified with distinct regions on the hydraulic map. Further, the laminar-to-turbulent transition and their respective entrance lengths arise as boundaries that demarcate classical regimes. These results may therefore be useful in educational contexts.

We also anticipate that our results will have practical applications in engineering settings as well as implications for the natural sciences. The formulas provided for the boundaries allow for quick identification of hydraulic regime and, if operating well away from the boundaries, simple and handy laws for the frictional resistance. If operating near any boundary, and especially for intermediate values of $Re \in [500, 5000]$ and $\alpha \in [10, 100]$, our model provides estimates that are significantly more accurate than any known law. Such predictions are likely to be particularly important for systems such as flow conditioners, piping manifolds, and filters that involve many parallel conduits, each perhaps short and of small individual resistance but whose sum yields a large net pressure drop. For the natural sciences, we foresee our model being useful for biological transport networks such as animal or plant vasculature. The Hagen–Poiseuille law is often used in modelling such networks despite violations of the requisite conditions on Re and α (Abadeh & Lew 2013; Jacobsen & Pratt 2018). We expect our model to provide a more accurate accounting of the hydraulics across the different length scales and flow rates in the branches at all levels of the network.

Our results apply strictly to specific geometric, driving and boundary conditions, and it is important to consider caveats and alternatives. We intend to characterize pipes that are smooth, straight, circular in cross-section, and of infinitesimal wall thickness. In such cases, length and diameter are the only geometric descriptors. An additional factor of

practical importance for many real pipes is wall roughness, whose effect for high aspect ratios (large α) is summarized in the famous Moody chart that shows increased resistance for turbulent flows in rough-walled pipes (Moody 1944). Further, our geometric ideal is questionable for very short pipes, whose hydraulics must in practice involve factors such as wall thickness and proximity to tank boundaries. Regarding driving conditions, our experimental system aims to impose a constant pressure differential across the pipe and measure the mean speed or flux after the flow is established. An alternative is to impose the rate and measure the pressure drop, which might be achieved experimentally with a syringe pump and pressure transducers. One expects correspondence with regard to time-averaged quantities insofar as the flow state is unique and the pressure-rate relation is single-valued and monotonic. The two schemes necessarily differ with regard to temporal fluctuations of pressure or rate for transitional and turbulent flows.

Regarding boundary conditions, our ideal inlet situation involves drawing from a large bath whose far-field flow can be assumed negligibly weak. Ambient flows present within any finite bath may contribute to the disturbances that trigger the laminar-to-turbulent transition, which may also be influenced by the edge geometry of the pipe inlet (Reynolds 1883). An alternative scheme imposes the velocity field at the inlet – as might be done with a syringe or piston in experiments, and with appropriate boundary conditions in simulations – in which case the entry flow, its acceleration and convergence into the pipe would be absent. A map applicable to such situations would not include the Torricelli regime. The outlet condition adopted here takes the form of a liquid jet into air. Alternatives include emptying into a large reservoir of liquid, e.g. a second tank of lower level, or suction via a syringe or piston. Exit effects are generally viewed as weak in comparison to the influence of the entrance, but these different outlet conditions may be significant for very short pipes and low Reynolds numbers (Green & Southard 2019).

As a first attempt at a universal formula for the friction function $f_D(Re, \alpha)$, our model presents many avenues for future developments, modifications and extensions. An overview of the main simplifying assumptions and parameter choices may motivate improvements. (1) For the inlet flows present in all cases, a single value of the discharge coefficient is used, whereas the function $C_D(Re, \alpha)$ varies in ways that are as yet incompletely characterized (Wu *et al.* 2002; Ferrante 2012; Hicks & Slaton 2014). (2) We demarcate the laminar and turbulent regimes with a purely mathematical prescription involving logistic functions, whereas an improved model might incorporate the physics of the flow transition (Moody 1944; Hof, Juel & Mullin 2003; White 2011). (3) A single constant for the friction factor is employed in the turbulent regime, whereas this is known to vary weakly with *Re* (Moody 1944; Nikuradse 1950; Langelandsvik *et al.* 2008; Adams *et al.* 2012). (4) The enhanced pressure drop due to development of laminar flow is modelled by an exponential function that is only roughly informed by known entrance flow phenomena (Sparrow *et al.* 1964; Langhaar 2021). (5) Development of turbulent flow is assumed to contribute no additional pressure drop, whereas the available evidence suggests that there may be a small influence (Barbin & Jones 1963; Wang & Tullis 1974). These issues further highlight the hidden complexities that can be involved in the seemingly simple act of drinking through a straw.

Declaration of interests. The authors report no conflict of interest.

Data availability statement. The data that support the findings of this study are openly available as a supplementary data file.

Author ORCIDs.

🄳 Olivia Pomerenk https://orcid.org/0000-0002-0481-3952;

🄳 Simon Carrillo Segura https://orcid.org/0000-0001-8287-5158;

🄳 Leif Ristroph https://orcid.org/0000-0001-9358-0689.

REFERENCES

ABADEH, A. & LEW, R.R. 2013 Mass flow and velocity profiles in *Neurospora* hyphae: partial plug flow dominates intra-hyphal transport. *Microbiology* **159** (11), 2386–2394.

ACHESON, D.J. 1991 *Elementary Fluid Dynamics*, 1st edn. Clarendon Press.

ADAMS, T., GRANT, C. & WATSON, H. 2012 A simple algorithm to relate measured surface roughness to equivalent sand-grain roughness. *Intl J. Mech. Engng Mechatron.* **1** (2), 66–71.

BARBIN, A.R. & JONES, J.B. 1963 Turbulent flow in the inlet region of a smooth pipe. *Trans. ASME J. Basic Engng* **85** (1), 29–33.

BATCHELOR, C.K. & BATCHELOR, G.K. 2000 *An Introduction to Fluid Dynamics*. Cambridge University Press.

BEN-DOV, G. & COHEN, J. 2007 Critical Reynolds number for a natural transition to turbulence in pipe flows. *Phys. Rev. Lett.* **98** (6), 064503.

BRKIĆ, D. & PRAKS, P. 2018 Unified friction formulation from laminar to fully rough turbulent flow. *Appl. Sci.* **8** (11), 2036.

CAMPBELL, W.D. & SLATTERY, J.C. 1963 Flow in the entrance of a tube. *Trans. ASME J. Fluids Engng* **85** (1), 41–45.

CHURCHILL, S.W. 1977 Comprehensive correlating equations for heat, mass and momentum transfer in fully developed flow in smooth tubes. *Ind. Engng Chem. Fundam.* **16** (1), 109–116.

COLEBROOK, C.F., BLENCH, T., CHATLEY, H., ESSEX, E.H., FINNIECOME, J.R., LACEY, G., WILLIAMSON, J. & MACDONALD, G.G. 1939 Correspondence, turbulent flow in pipes, with particular reference to the transition region between the smooth and rough pipe laws. *J. Inst. Civ. Engrs* **12** (8), 393–422.

CURTIS, W.D., LOGAN, J.D. & PARKER, W.A. 1982 Dimensional analysis and the pi theorem. *Linear Algebra Appl.* **47**, 117–126.

DOMBROWSKI, N., FOUMENY, E.A., OOKAWARA, S. & RIZA, A. 1993 The influence of Reynolds number on the entry length and pressure drop for laminar pipe flow. *Can. J. Chem. Engng* **71** (3), 472–476.

DRAAD, A.A., KUIKEN, G.D.C. & NIEUWSTADT, F.T.M. 1998 Laminar–turbulent transition in pipe flow for Newtonian and non-Newtonian fluids. *J. Fluid Mech.* **377**, 267–312.

EISENBURGER, M. & ADDY, M. 2003 Influence of liquid temperature and flow rate on enamel erosion and surface softening. *J. Oral Rehabil.* **30** (11), 1076–1080.

FARGIE, D. & MARTIN, B.W. 1971 Developing laminar flow in a pipe of circular cross-section. *Proc. R. Soc. Lond.* A **321** (1547), 461–476.

FERRANTE, M. 2012 Experimental investigation of the effects of pipe material on the leak head-discharge relationship. *ASCE J. Hydraul. Engng* **138** (8), 736–743.

GREEN, D.W. & SOUTHARD, M.Z. 2019 *Perry's Chemical Engineers' Handbook*. McGraw-Hill Education.

HICKS, A. & SLATON, W. 2014 Determining the coefficient of discharge for a draining container. *Phys. Teacher* **52** (1), 43–47.

HOF, B., JUEL, A. & MULLIN, T. 2003 Scaling of the turbulence transition threshold in a pipe. *Phys. Rev. Lett.* **91** (24), 244502.

JACOBSEN, A.L. & PRATT, R.B. 2018 Going with the flow: structural determinants of vascular tissue transport efficiency and safety. *Plant Cell Environ.* **41** (12), 2715–2717.

KERSWELL, R.R. 2005 Recent progress in understanding the transition to turbulence in a pipe. *Nonlinearity* **18** (6), R17.

KIM, W. & BUSH, J.W.M. 2012 Natural drinking strategies. *J. Fluid Mech.* **705**, 7–25.

LANGELANDSVIK, L.I., KUNKEL, G.J. & SMITS, A.J. 2008 Flow in a commercial steel pipe. *J. Fluid Mech.* **595**, 323–339.

LANGHAAR, H.L. 2021 Steady flow in the transition length of a straight tube. *J. Appl. Mech.* **9** (2), A55–A58.

MALCHEREK, A. 2016 History of the Torricelli principle and a new outflow theory. *ASCE J. Hydraul. Engng* **142** (11), 02516004.

MOODY, L.F. 1944 Friction factors for pipe flow. *Trans. ASME* **66**, 671–684.

MULLIN, T. 2011 Experimental studies of transition to turbulence in a pipe. *Annu. Rev. Fluid Mech.* **43**, 1–24.

NIKURADSE, J. 1950 Laws of flow in rough pipes. *Tech. Rep.* 1292. National Advisory Committee for Aeronautics.

NILSSON, H., EKBERG, O., OLSSON, R., KJELLIN, O. & HINDFELT, B. 1996 Quantitative assessment of swallowing in healthy adults. *Dysphagia* **11** (2), 110–116.

PICKOVER, C. 2008 *Archimedes to Hawking: Laws of Science and the Great Minds Behind Them*. Oxford University Press.

REYNOLDS, O. 1883 XXIX. An experimental investigation of the circumstances which determine whether the motion of water shall be direct or sinuous, and of the law of resistance in parallel channels. *Phil. Trans. R. Soc. Lond.* **174**, 935–982.

SEMAT, H. & KATZ, R. 1958 *Physics*. Rinehart & Company.

SPARROW, E.M., LIN, S.H. & LUNDGREN, T.S. 1964 Flow development in the hydrodynamic entrance region of tubes and ducts. *Phys. Fluids* **7**, 338–347.

STOKES, G.G. 1845 On the theories of the internal friction of fluids in motion, and of the equilibrium and motion of elastic solids. *Trans. Camb. Phil. Soc.* **8**, 287–341.

VOGEL, S. 2013 *Comparative Biomechanics: Life's Physical World*. Princeton University Press.

WANG, J.-S. & TULLIS, J.P. 1974 Turbulent flow in the entry region of a rough pipe. *Trans. ASME J. Fluids Engng* **96** (1), 62–68.

WHITE, F.M. 2011 *Fluid Mechanics*. McGraw-Hill.

WU, D., BURTON, R. & SCHOENAU, G. 2002 An empirical discharge coefficient model for orifice flow. *Intl J. Fluid Power* **3** (3), 13–19.